Title

Cobalt-Doped Black TiO2 Nanotube Array as a Stable Anode for Oxygen Evolution and Electrochemical Wastewater Treatment

Journal

ACS Catalysis, 8(5)

ISSN

2155-5435

Authors

Yang, Yang
Kao, Li Cheng
Liu, Yuanyue
et al.

Publication Date

2018-05-04

DOI

10.1021/acscatal.7b04340

Peer reviewed

ACS Catalysis

Research Article

Cite This: ACS Catal. 2018, 8, 4278–4287

pubs.acs.org/acscatalysis

Cobalt-Doped Black TiO_2 Nanotube Array as a Stable Anode for Oxygen Evolution and Electrochemical Wastewater Treatment

Yang Yang,[†] Li Cheng Kao,[‡] Yuanyue Liu,[§] Ke Sun,[∥] Hongtao Yu,[⊥] Jinghua Guo,[#,▽] Sofia Ya Hsuan Liou,[‡] and Michael R. Hoffmann*[,†]

[†]Division of Engineering and Applied Science, Linde-Robinson Laboratory, California Institute of Technology, Pasadena, California 91125, United States

[‡]Department of Geosciences, National Taiwan University, P.O. Box 13-318, Taipei 106, Taiwan

[§]Department of Mechanical Engineering and Texas Materials Institute, University of Texas at Austin, Austin, Texas 78712, United States

[∥]Divisions of Chemistry and Chemical Engineering, California Institute of Technology, Pasadena, California 91125, United States

[⊥]School of Environmental Science and Technology, Dalian University of Technology, Dalian 116024, People's Republic of China

[#]Advanced Light Source, Lawrence Berkeley National Laboratory, Berkeley, California 94720, United States

[▽]Department of Chemistry and Biochemistry, University of California, Santa Cruz, California 95064, United States

Supporting Information

ABSTRACT: TiO_2 has long been recognized as a stable and reusable photocatalyst for water splitting and pollution control. However, it is an inefficient anode material in the absence of photoactivation due to its low electron conductivity. To overcome this limitation, a series of conductive TiO_2 nanotube array electrodes have been developed. Even though nanotube arrays are effective for electrochemical oxidation initially, deactivation is often observed within a few hours. To overcome the problem of deactivation, we have synthesized cobalt-doped Black-TiO_2 nanotube array (Co-Black NTA) electrodes that are stable for more than 200 h of continuous operation in a $NaClO_4$ electrolyte at 10 mA cm^{-2}. Using X-ray photoelectron spectroscopy, X-ray absorption spectroscopy, electron paramagnetic resonance spectroscopy, and DFT simulations, we are able to show that bulk oxygen vacancies (O_v) are the primary source of the enhanced conductivity of Co-Black. Cobalt doping both creates and stabilizes surficial oxygen vacancies, O_v, and thus prevents surface passivation. The Co-Black electrodes outperform dimensionally stable IrO_2 anodes (DSA) in the electrolytic oxidation of organic-rich wastewater. Increasing the loading of Co leads to the formation of a CoO_x film on top of Co-Black electrode. The CoO_x/Co-Black composite electrode was found to have a lower OER overpotential (352 mV) in comparison to a DSA IrO_2 (434 mV) electrode and a stability that is greater than 200 h in a 1.0 M KOH electrolyte at a current density of 10 mA cm^{-2}.

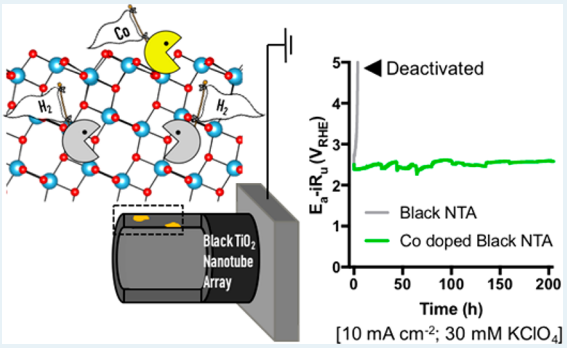

KEYWORDS: *conductive TiO_2 nanotube array, cobalt oxide, oxygen vacancies, oxygen evolution reaction, wastewater treatment*

INTRODUCTION

TiO_2 has long been recognized as a stable and reusable photocatalyst for water splitting and pollution.[1] However, potential applications of TiO_2 are most often correlated with its oxygen evolution reaction (OER) potential.[1,2] In spite of success in laboratory-scale research, many challenges remain with respect to the use of TiO_2 in solar fuel production and environmental remediation due to (1) its high band-gap energy of 3.2 eV (i.e., 385 nm) and (2) high attenuation coefficients for the penetration of incident UV photons in turbid water (i.e., both freshwater and wastewater). Some of these intrinsic barriers can be overcome when TiO_2 is used in electrochemical systems applications without the need for direct photoactivation of TiO_2.[3,4] However, the low mobile carrier conductivity of n-type TiO_2 impedes its use as an electrocatalyst. The transport of electrons across the electrolyte/TiO_2 interface requires a large anodic potential (>3 $V_{Ag/AgCl}$) to overcome a high Schottky barrier.[4]

The electronic properties of TiO_2 can be tuned by self-doping. It is known that H_2 reduction could introduce Ti^{3+}, oxygen vacancies, and surface disorders to TiO_2. The resultant Black TiO_2 has a narrower band gap.[5−7] Black TiO_2 catalysts on both anatase and rutile structures exhibited high activity in visible-light-driven water oxidation.[8,9] However, their activity

Received: December 18, 2017
Revised: April 9, 2018
Published: April 10, 2018

DOI: 10.1021/acscatal.7b04340
ACS Catal. 2018, 8, 4278−4287

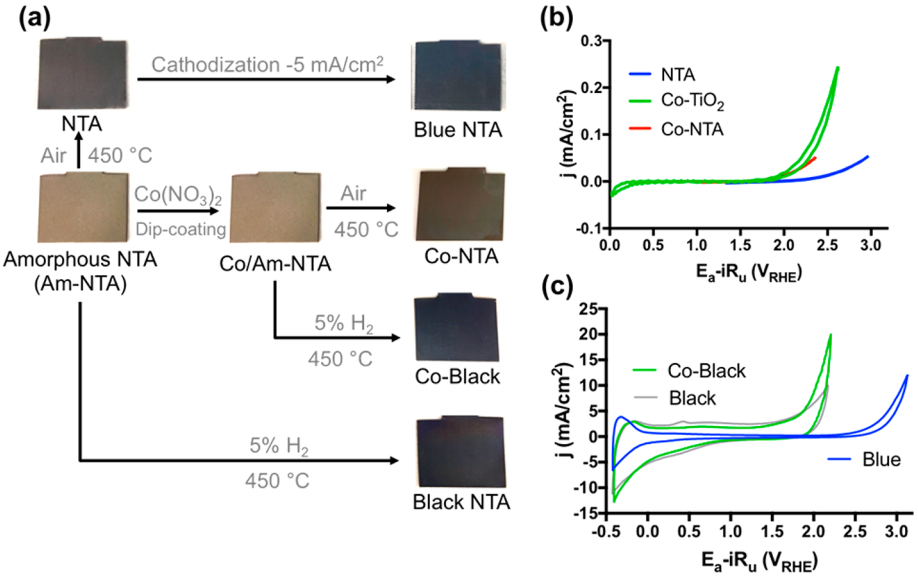

Figure 1. (a) NTA electrode preparation procedures. (b, c) Cyclic voltammograms of NTA electrodes in 100 mM KPi buffer at pH 7.2.

during dark electrolysis has been less explored. Reducing TiO_2 in pure H_2 at temperatures over 1000 °C promotes the bulk phase transition from anatase to substoichiometric Magnéli phase Ti_4O_7.[10] Magnéli phase TiO_2 has conductivities that approach 11 orders of magnitude greater than that of TiO_2.[11] Thus, it has been shown to be a stable anode material for water oxidation and wastewater treatment.[12,13]

Given that the preparation of Ti_4O_7 requires highly reducing conditions, it is often difficult to prepare conductive, stoichiometric TiO_2 using conventional techniques. Recently, conductive TiO_2 nanotube arrays (NTAs) that are either blue or black in appearance have been reported. Black NTAs were prepared by reducing anatase NTA under an H_2 or H_2/Ar atmosphere at 450−550 °C.[14,15] Blue NTAs were obtained by cathodization of anatase NTA in aqueous electrolyte.[16−20] Conductive NTA electrodes have satisfactory electrochemical oxidation activity.[20,21] The synthetic preparation procedures for Blue and Black NTA are less stringent than those of the Magnéli phases, Ti_xO_{2x-1}.

Conductive NTAs supported on titanium plates have a major advantage over particulate electrocatalysts, since they can be utilized directly as electrodes without the need for additional adhesive substrates or organic binders. However, deactivation of both Blue and Black NTAs has been observed after a few hours of electrocatalysis due to the surface passivation.[20,21] Therefore, electrodes made from these materials are currently impractical for engineering applications.

In this study, we report on the effect of doping trace amounts of cobalt onto Black TiO_2 NTA (Co-Black NTA) that results in a lowering of the OER overpotential and increases electrode stability. Even though bulk CoO_x is reported to be unstable for the OER at pH <12 in phosphate-free electrolyte solutions,[22,23] we observe that CoO_x is immobilized and stable on Black NTAs even at circumneutral pH. We show that Co-Black electrodes outperform an IrO_2-based dimensionally stable anode (DSA) for oxidative electrochemical wastewater treatment. We also found that the increase of Co loading forms a CoO_x film on top of Co-Black substrate. The resultant CoO_x/Co-Black composite electrode exhibits high OER activity (overpotential of 352 mV vs 434 mV for IrO_2 DSA) and stability (>200 h) in 1 M KOH electrolyte at 10 mA cm^{-2}.

EXPERIMENTAL SECTION

Electrode Preparation. The overall approach to synthesize NTA electrodes is schematically illustrated in Figure 1a. Amorphous TiO_2 NTA (Am-NTA) was prepared by anodization of a Ti plate (6 cm^2, 0.5 mm) at 42 V in ethylene glycol (EG) electrolyte with 0.25 wt % NH_4F and 2 wt % H_2O for 6 h.[24] After anodization, Am-NTA was subjected to a second anodization in 5 wt % H_3PO_4/EG electrolyte at 42 V for 1 h to enhance its mechanical stability.[20,25]

Cobalt-loaded Am-NTA (Co/Am-NTA) was prepared by dipping Am-NTA into 250 mM $Co(NO_3)_2$/ethanol solution. The sample was dipped into the coating solution for 1 min, pulled up at the rate of 10 mm/min, and finally dried at room temperature for 2 min. The dip-coating processes were repeated three times. The Co loading was determined by ICP-MS (Agilent 8800) as 0.54 ± 0.12 μmol/cm^2. Lowering the $Co(NO_3)_2$ concentration in the dip-coating solutions to 50 and 25 mM produced Co(0.25)- and Co(0.17)-Black NTA with Co loadings of 0.25 and 0.17 μmol/cm^2, respectively.

Annealing Am-NTA and Co/Am-NTA in air at 450 °C for 1 h yieldeds NTA and Co-NTA, respectively. Black NTA and Co-doped Black NTA (Co-Black) were obtained by annealing Am-NTA and Co/Am-NTA in a stream of 5% H_2/Ar at 450 °C for 30 min and then naturally cooling to room temperature. The Blue NTA was prepared by applying a cathodic current of 5 mA cm^{-2} on the NTA electrode for 10 min in 0.1 M potassium phosphate buffer solution (KPi). All of the thermally treated NTAs were determined to be in the anatase phase by XRD (Figure S1). Five control samples were prepared. (1) A cobalt-doped TiO_2 (Co-TiO_2) film electrode was prepared by spray-coating a mixture of 250 mM titanium−glycolate complex and 25 mM $Co(NO_3)_2$ onto a Ti plate, followed by annealing in air at 450 °C for 1 h.[26] The final mass loading of Co-TiO_2 was 6 mg/cm^2. The molar Co loading was 0.6 μmol/cm^2. (2) Amorphous cobalt hydroxide was loaded onto a Ti plate ($Co(OH)_x$/Ti) by the electrochemical deposition method described previously,[27] with the modification of replacing the glassy-carbon substrate with a titanium plate. (3) Cobalt oxide was coated onto the Ti plate (CoO_x/Ti) by a drop-casting method using 250 mM $Co(NO_3)$ in ethanol as precursor,

DOI: 10.1021/acscatal.7b04340
ACS Catal. 2018, 8, 4278−4287

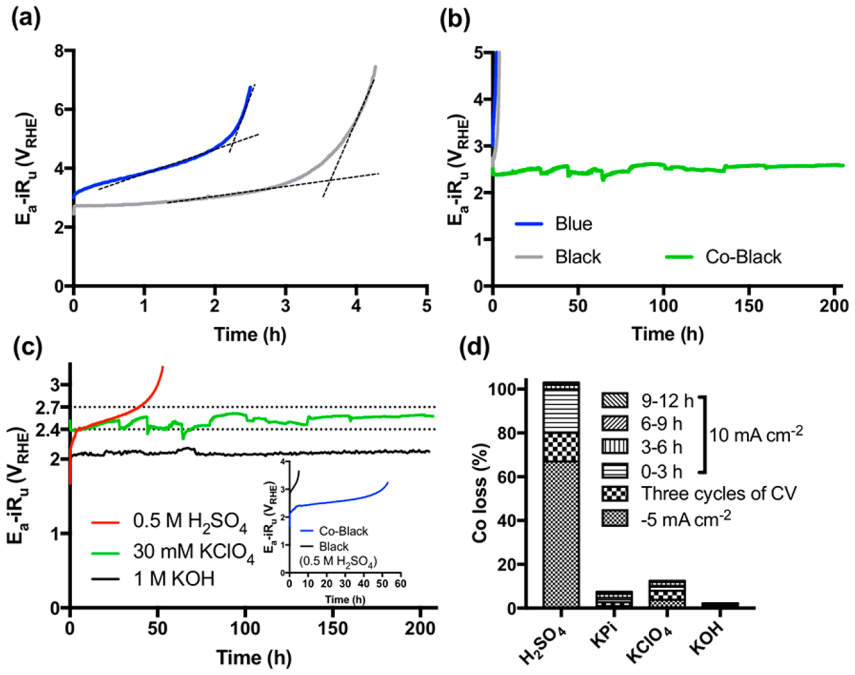

Figure 2. (a, b) Comparison of the anodic stability of the NTA electrodes in 30 mM $KClO_4$ at a current density of 10 mA cm^{-2}. (c) Effect of the composition of the electrolytes on anodic stability (insert: comparison of stability of Co-Black NTA and Black NTA in 0.5 M H_2SO_4). (d) Effect of electrolyte composition on cobalt leaching from the NTA electrode material.

followed by annealing under 5% H_2/Ar at 450 °C for 30 min. (4) IrO_2 DSA anodes were prepared by spray-coating an $IrCl_3$/isopropyl alcohol solution onto a hot Ti plate (6 cm^2, 0.5 mm) at 300 °C, followed by annealing at 450 °C for 1 h.[26] The mass loading of IrO_2 was 0.5 mg cm^{-2}. (5) Commercial IrO_2 DSA (C-DSA) was purchased from Nanopac, Korea.

Catalyst Characterization. Cyclic voltammetry (CV) and electrochemical impedance spectroscopy (EIS) were measured using a Biologic VSP-300 potentiostat. Uncompensated resistance (R_u) was measured by EIS. All of the presented anodic potentials were corrected by R_u. EIS was also used to determine Mott−Schottky plots. These details are described in Text S2 of the Supporting Information. For two-point solid-state measurements, nanotube tops were contacted by sputter-evaporated 10 nm thick Au using a Cressington 208HR sputter coater. Then resistance was obtained from the $I-V$ curves collected by potentiostat.

After CV analyses, NTA electrodes were characterized by scanning electron microscopy (SEM, ZEISS 1550VP) coupled with energy dispersive X-ray spectroscopy (EDS), scanning transmission electron microscopy (STEM, FEI TF30ST) equipped with a high angle annular dark field (HAADF) detector, X-ray photoelectron spectroscopy (XPS) with Surface Science M-Probe ESCA/XPS, and X-ray diffractometry (PANalytical X'Pert Pro). Electron paramagnetic resonance spectra were collected on a Bruker EMX X-band CW-EPR spectrometer at room temperature and 10 K. Powder samples were collected by scraping NTA from the Ti metal substrate.

X-ray Absorption Spectroscopy. X-ray absorption spectroscopy (XAS) of Ti L-edge and O K-edge were measured on Beamline 8.0.1 at the Advanced Light Source (ALS), Lawrence Berkeley National Laboratory. The resolutions of the measurements were 0.4 eV at the O K-edge and 0.3 eV at the Ti L-edge. Spectra were recorded in total electron yield mode (TEY) and were obtained by measurement of the sample drain photocurrent under irradiation with monochromatic light. The XAS at Co K-edge was conducted at BL17C1 at the National Synchrotron Radiation Research Center, Taiwan. The photon energy calibrations of the XAS spectra at the Ti L-edge and O K-edge were conducted on the basis of the reference anatase TiO_2 films. The incident radiation flux was monitored by the photocurrent produced in a gold mesh in the beam path. All spectra were normalized to the incident flux recorded with Au mesh.

Cobalt Leaching and Anodic Stability Testing. The Co-Black NTA electrodes were subjected to cathodization (−5 mA/cm^2, 10 min), CV (−0.5 to +3 V_{RHE}, 10 mV s^{-1}), and four continuous stages of constant current electrolysis (10 mA cm^{-2}) at an interval of 3 h. At the end of each step, a water sample was collected, acidified by HNO_3, and then analyzed by ICP-MS (Agilent 8800) to determine the Co concentration. The electrolyte was replaced before the next test. The anodic stability test was performed following the constant current Co leaching test. Current density was maintained at 10 mA cm^{-2}. Electrolyte was replaced every 12 h.

OER, CER, and Water Treatment Tests. OER activities were evaluated using Tafel plots, which were collected by potentiostat with a three-electrode configuration. Stainless steel and saturated Ag/AgCl were used as counter and reference electrodes, respectively. Data were collected at constant current mode (0.01−10 mA cm^{-2}). Each current step was maintained for 5 min to measure the steady-state anodic potential.

Hydroxyl radical production and direct electron transfer activities were measured using benzoic acid and oxalate as probe molecules, respectively. Benzoic acid was measured by HPLC (Agilent 1100) equipped with a Zorbax XDB column. Oxalate was analyzed by ion chromatography (ICS 2000, Dionex). Free chlorine concentrations ([FC]) were measured using the DPD (*N*,*N*-diethyl-*p*-phenylenediamine) reagent (Hach method 10102). The current efficiency was estimated using the equation

DOI: 10.1021/acscatal.7b04340
ACS Catal. 2018, 8, 4278−4287

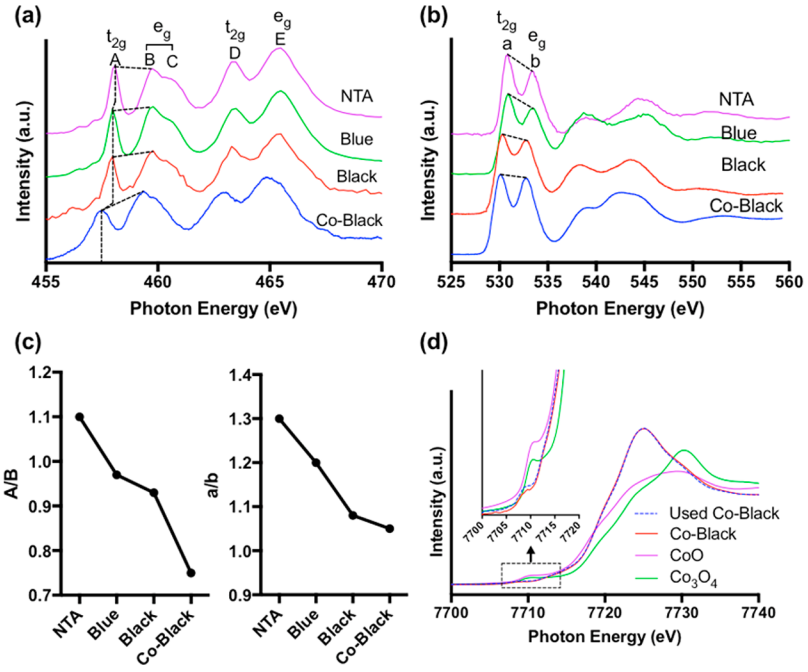

Figure 3. (a) Ti L-edge, (b) O K-edge XAS spectra, and (c) intensity ratio of specific peaks. (d) Co K-edge XAS spectra (insert: enlarged view of pre-edge structure).

$$\eta = \frac{2VF\ \mathrm{d[FC]}}{I\ \mathrm{d}t} \quad (1)$$

where V is electrolyte volume (25 mL), F is the Faraday constant (96485 C mol^{-1}), and I is the current (A). Chemical oxygen demand (COD) in wastewater was determined by the dichromate digestion method (Hach Method 8000). NH_4^+ was quantified by ion chromatography.

Latrine wastewater was collected from a recycling electrochemical toilet system located on the Caltech campus (Pasadena, CA). The latrine wastewater has a pH of around 8.5 with a conductivity of 13.5 mS cm^{-1}. It contains 500 mg L^{-1} COD and 18.5 mM NH_4^+. During the electrolysis of latrine wastewater, the Co-Black and IrO_2 electrodes were operated at 10 mA cm^{-2} with cell voltages of 4.6 and 4 V, respectively. The electrode area/wastewater volume ratio was set as 60 m^{-1}.

RESULTS AND DISCUSSION

The electrochemical activity of electrodes was determined by cyclic voltammetry (CV) in potassium dihydrogen phosphate (KPi) buffer solutions. The anodic branch current response is due to the OER. Both NTA and Co-NTA have low OER activity, as indicated by the low current densities of Figure 1b. The Co-TiO_2 film electrode has higher current response in comparison to NTA and Co-NTA, but its performance is inferior to that of conductive NTA electrodes (Figure 1b vs Figure 1c). An increase in current response is observed on both the Blue and Black NTA electrodes at onset potentials of 2.7 and 1.7 V, respectively (Figure 1c). Co-Black NTA has the highest OER activity due to its lower onset potential and its higher current density. There have been previous reports that Co-doped TiO_2 nanotubes could be used as photoelectrochemical water-splitting catalysts.[28−31] However, their photocurrent densities are less than 5 mA/cm^2. In a recent report, Co_3O_4/TiO_2 nanotubes were used for dark water electrolysis.[32] However, it appeared that TiO_2 functioned only as an inert substrate for Co_3O_4 with resulting current densities <1 mA/cm^2 at an applied potential of 2.3 V_{RHE}. These results are in agreement with the inert performance observed on a Co-TiO_2 film electrode with 0.6 μmol/cm^2 Co loading prepared in this study. In contrast, Co-Black NTA with less Co loading (0.54 μmol/cm^2) exhibits 200 times higher current density in comparison with a Co-TiO_2 film electrode at 2.3 V_{RHE}. This finding highlights the promotional role of conductive NTA substrate on the OER activity of Co-TiO_2 system.

The anodic stability of the NTA electrodes at circumneutral pH was determined by applying a constant current of 10 mA cm^{-2} in a $KClO_4$ electrolyte solution. Deactivation of the electrode was determined from the sharp increase in anodic potential (Figure 2a). The Blue and Black NTAs have lifetimes of 2.3 and 4 h, respectively, which are in line with previous studies.[20,21] A substantially longer lifetime and apparent stability (>200 h) were observed for the Co-Black NTA electrode (Figure 2b). Lowering the Co loading to 0.25 and 0.17 μmol/cm^2 does not affect the stability of Co-Black NTA within the investigated 100 h electrolysis (Figure S2a). The results suggest that a trace amount of the Co dopant is sufficient to significantly enhance the stability of Black NTA.

Figure 2c shows that the Co-Black electrode is also stable in 1.0 M KOH. However, deactivation occurs after 45 h in 0.5 M H_2SO_4. Nevertheless, Co-Black electrode still has a longer lifetime than Black NTA (insert of Figure 2c). We further investigated the leaching of Co in different electrolytes at cathodic (−5 mA cm^{-2}), fluctuating (CV), and anodic (10 mA cm^{-2}) currents (Figure 2d). Complete dissolution of Co from Co-Black was observed after sequential cathodization, CV, and 12 h electrolysis in H_2SO_4. In contrast, only 2.1% of Co was lost under similar conditions in the KOH electrolyte. Retarded Co leaching is also observed in the 0.1 M KPi electrolyte; this is probably due to the formation of less soluble CoPi.[33,34] In addition, the leaching of Co from Co-Black is undetectable (<0.03%) by ICP-MS after 9 h of electrolysis in $KClO_4$ in the absence of phosphate. Analyses by SEM-EDS and STEM-HAADF indicate that Co is well dispersed in Co-rich spots on

DOI: 10.1021/acscatal.7b04340
ACS Catal. 2018, 8, 4278−4287

Co-Black throughout the tube length. CoO_x particles were not found (Figures S3−S6).

Two-point solid-state conductivity measurements show that the resistances of Blue, Black, and Co-Black NTA electrodes are 5 orders of magnitude lower than that of pristine NTA electrodes (Figure S7). Knowing that the above measurements may be interfered by the contact resistance of Au coating, we further probed the semimetallic properties of conductive NTA by EIS using liquid electrolyte contacts (Figure S8). The Blue, Black, and Co-Black NTA all have good conductivity, but their OER activities vary. This implies that, in addition to bulk conductivity considerations, surface specific characteristics need to be considered.

Both electrochemical and thermal reduction should promote the formation of Ti^{3+} sites and adjacent oxygen vacancies (O_vs) on TiO_2. However, aside from Ti^{4+}, X-ray photoelectron spectroscopy (XPS) cannot confirm the existence of Ti^{3+} on Blue and Black NTA, probably due to the reoxidation of Ti^{3+} to Ti^{4+} in ambient air (Figure S9). Nevertheless, the oxidation of Ti^{3+} is essentially the filling of O_v by adsorbed oxygen species, which can be detected by XPS (Figure S10). The relative concentration of absorbed oxygen species is associated with the abundance of nascent O_v. The XPS O 1s spectrum reveals that the concentration of oxygen vacancies (O_v) decreases in the order Black (22%) > Blue (17%) > pristine NTA (12%). XPS analyses also found that Co doping results in a significant reduction in the Ti oxidation state in Co-Black NTA and creates more surficial O_v (25%) (Figures S9 and S10).

The NTA samples were further investigated using X-ray absorption spectroscopy (XAS) operated in total electron yield (TEY) mode. The results obtained from TEY mode involved both surface and subsurface characteristics, as XAS has a larger sampling depth in comparison to XPS. The Ti L-edge XAS is shown in Figure 3a. The spectra that result from the transition of electrons from the Ti $2p_{3/2}$ and $2p_{1/2}$ initial states to the unoccupied 3d orbital. Peaks A−C correspond to the electronic transition from $2p_{3/2}$ to 3d, while peaks D and E can be assigned to the transition from $2p_{1/2}$ to 3d.[35] The single crystal of TiO_2 has octahedral (O_h) symmetry. The O_h crystal field splits the Ti 3d band into t_{2g} and e_g degenerate orbitals. The excitation of electrons from the ground state of Ti^{4+} to t_{2g} orbital can be expressed as $2p^63d^0 \rightarrow 2p^53d^1$, which is reflected as the energy absorption at 458 eV (peak A). Ti^{3+} ($2p^63d^1$) already has one electron in the t_{2g} orbital, which reduces the number of unoccupied states. Therefore, the presence of Ti^{3+} leads to the reduction of t_{2g} relative intensity and e_g peak width broadening.[35] The lesser resolved peaks B and C, the reduction of the A/B intensity ratio (Figure 3c), and the shift of peak A to lower energy confirm the presence of Ti^{3+} in Blue and Black NTA as well.[35,36] The O K-edge XAS is shown in Figure 3b. Peaks a and b can be assigned to the electronic transition from O 1s to O 2p hybridized with the Ti 3d t_{2g} and 3d e_g states, respectively.[37,38] The peak intensity ratio of t_{2g} to e_g is lower in Blue and Black NTA (Figure 3c), which suggests the presence of more Ti^{3+} and O_v.[35] In agreement with the XPS analyses, Co-Black has the highest number of Ti^{3+} and O_v, sites as supported by the lowest peak A/B and a/b ratios in XAS (Figure 3c).

We further investigated the oxidation state and coordination environment of Co dopant by XAS. The absorption edge in Co K-edge XAS spectra of Co-Black overlaps with that of CoO (Figure 3d); this implies that surficial Co ions of Co-Black are in valence 2+, which is in line with the XPS analyses (Figure S9), and the EPR results (vide infra). The pre-edge peaks of CoO and Co_3O_4 correspond to the 1s−3d electronic transitions contributed by the tetrahedrally coordinated Co^{2+}. This feature is less pronounced for Co-Black, indicating that Co^{2+} is in an O_h configuration in which 1s−3d electronic transitions rarely occur.[39] The overall Co K-edge profile of Co-Black is different from that of CoO and Co_3O_4. This results again suggest that the coordination structure of Co^{2+} ions in Co-Black is clearly different from that of oxide particles. Given that no CoO_x particulates could be found by both SEM and TEM, it is possible that Co^{2+} is atomically doped into the lattice of TiO_2, adopting the same O_h configuration. This assumption needs to be verified by aberration-corrected TEM in a future study.

The coordination structure of Co^{2+} remains intact after 100 h of electrolysis, as indicated by the unchanged Co K-edge profiles of Co-Black before and after use (Figure 3d). Of note, XPS data indicated that Co^{2+} in Co-NTA was prepared by annealing the $Co(NO_3)_2$ loaded Am-NTA in air, even though the calcination of $Co(NO_3)_2$ alone produced Co_3O_4 (i.e., a mixed Co(III)/Co(II) material). (Figure S9). These observations combined suggest that Co^{2+} is effectively immobilized on NTA and its reduced valence state does not result from H_2 reduction but from a strong Co−TiO_2 interaction. It is noteworthy that Co^{2+} in CoO_x is a labile OER intermediate that tends to be dissolved at neutral pH in the absence of phosphate.[23,33] Our findings suggest that the Co−TiO_2 interaction is strong enough to prevent Co leaching at circumneutral pH. These results could provide a new strategy to prepare stable CoO_x-based OER catalysts.

NTA samples were scraped off from Ti substrate for EPR characterization. The EPR signals of powdered NTA samples should mainly reflect their bulk characteristics. Signals were normalized by sample weight in order to perform semi-quantitative comparison. The EPR signal at a g value of 2.003 could be attributed to electrons localized on O_v.[14,40] As shown above, XPS and XAS unambiguously point out that Blue NTA has more surficial O_v than pristine NTA. However, higher bulk phase O_v concentration is not observed on Blue NTA, as shown by EPR (Figure 4a), implying that electrochemical reduction only results in changes on the surface/subsurface of Blue NTA. The results seem to be reasonable, since the mild electrochemical reduction that was carried out at room temperature is less likely to dislodge bulk lattice oxygen. In contrast, H_2-assisted thermal reduction largely increases the bulk O_v concentration of Black NTA, which is reflected as an 80 times increase in peak intensity in the EPR spectrum (Figure 4b).

In comparison with Black NTA, Co-Black has an O_v signal with lower intensity (Figure 4b). However, such a discrepancy is eliminated in EPR spectra recorded at 10 K (Figure 4c). In addition, Co-Black shows an EPR signal at g = 4.2, which could be assigned to high-spin (S = 3/2) Co^{2+} in an O_h environment.[41] The results combined imply (1) the bulk O_v concentration of Co-Black NTA is commensurate with that of Black NTA and (2) the Co^{2+} centers enhance relaxation of unpaired electrons of neighboring O_v sites. As a consequence, the O_v resonance signal of Co-Black is attenuated at room temperature. As shown in the inset of Figure 4c, resonance signals at g = 1.92, which can be attributed to Ti^{3+},[42] were observed on both Black and Co-Black NTA. The Co-Black NTA has more Ti^{3+} sites, resulting in a higher signal intensity.

The Ti^{3+}−O_v pairs serve as electron donors to facilitate bulk conductivity. Thus, the elevated conductivity of Black NTA and

DOI: 10.1021/acscatal.7b04340
ACS Catal. 2018, 8, 4278−4287

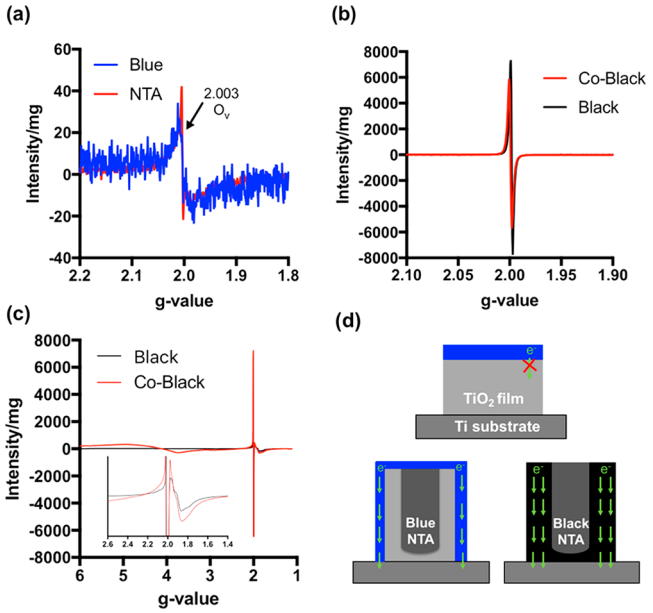

Figure 4. EPR spectra recorded at (a, b) room temperature and (c) 4 K (inset: the enlarged area at a *g* value of 1.4−2.6). (d) Schematic illustrations of electron conduction mechanisms.

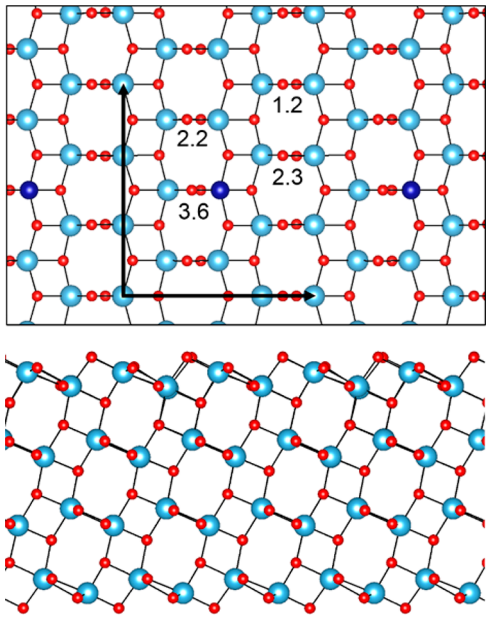

Figure 5. Atomic models of the TiO_2 (101) surface in top view (top panel) and side view (bottom panel). Color code: cyan, Ti; red, O; blue, Co. The black lines indicate the vectors of the surface supercell. The numbers show the magnitude of the relative formation energy of the corresponding oxygen vacancy.

Co-Black NTA in comparison with pristine NTA can be assigned to the increase in bulk O_v concentration (Figure 4d). For the Blue NTA, the mechanism seems to be more complicated. It is suspected that electrochemical reduction only makes the surface/subsurface of Blue NTA conductive. Thanks to its vertically aligned tubular structure, electrons are able to transfer to the Ti substrate through the "conductive skin" of Blue NTA. In contrast, as we proved previously, the TiO_2 film electrode without such a structure cannot gain anodic conductivity after electrochemical reduction,[20] probably due to the presence of underlying, insulating bulk TiO_2.

Good conductivity is a prerequisite for electrocatalysts, while their catalytic activity is determined by the number of active sites. The surficial O_v is generally considered as an active site for the OER.[43,44] It exposes unsaturated metal ions, which in turn lead to the adsorption and dissociation of H_2O.[45,46] Black NTA has more surficial O_v sites and thus has a lower onset potential for the OER and a correspondingly higher activity in comparison to the Blue NTA. Clearly, the highest observed OER activity of Co-Black NTA electrodes can be attributed to the higher abundance of O_v. The pristine NTA also has surficial O_v, but the lack of bulk O_v impedes bulk phase electron transport. As a consequence, pristine NTA has no discernible OER activity. The same rule can be invoked to explain the inert OER activity of Co-NTA and Co-TiO_2 film electrode (Figure 1b).

Computational simulation using density functional theory (DFT) was performed to provide insight into the mechanism of Co−TiO_2 interactions at an atomic level (detail can be found in Text S1). Simulations were focused on the TiO_2 (101) plane because (1) as observed by HRTEM (Figure S5a), the tube wall is mainly composed of (101) plane, which in line with the observation of a previous study,[47] and (2) XRD analyses show that the (101) plane is sensitive to surface fabrication, as the Co doping only affects the crystallinity of the (101) plane, while other planes remain intact (Figure S1). The DFT simulation found that O_v formation is more favorable by 3.6 eV when the neighboring Ti is substituted by Co (Figure 5). This is because Co forms a weaker bond with O in comparison to Ti, as reflected in the formation energy of TiO_2 (−3.5 eV atom^{-1}) in comparison to the Co oxides (Co_3O_4, −1.4 eV atom^{-1}; CoO, −1.3 eV atom^{-1}; CoO_2, −1.1 eV atom^{-1}).[48] The simulation also shows that the O atoms which are not directly bonded to Co tend to form vacancies as well, indicating a nonlocal effect. Since the formation of O_v reduces the coordination of the metal ions, the apparent oxidation states should be lower than those sites in the pristine material. This interpretation is in line with the reduced Ti and Co valence states in Co-Black.

The results of the DFT simulation imply that Co doping could thermodynamically stabilize surficial O_v. This mechanism has a significant effect on electrode lifetime. For both Blue and Black NTA, deactivation could be ascribed to surface passivation due to the irreversible uptake of oxygen and subsequent loss of O_v during prolonged OER. As shown in Figure 6, a reduction in the O_v concentration from 22% to 16% was found on Black NTA after deactivation, while such a change could not be observed on Co-Black. The hypothesis presented above may explain the superior stability of Co-Black in comparison to Black NTA in H_2SO_4 electrolyte solutions (insert of Figure 2c). The leaching of Co from Co-Black under acidic conditions may create additional O_vs, which in turn enables Co-Black to have a longer lifetime than Black NTA. However, the newly formed O_vs will not be stabilized by Co due to its loss via leaching from the Co-Black NTA matrix. Therefore, the deactivation will take place over time under acidic conditions.

Two OER catalysts, nickel oxides and iron oxides, were loaded on Black NTA electrodes by dip coating. It is found that Ni-Black and Fe-Black NTA electrodes exhibit improved stability in comparison with Black NTA but they still suffered from deactivation after 40 h of electrolysis in $KClO_4$ electrolyte (Figure S2a). No residual Ni and Fe could be detected on the deactivated electrodes, indicating the complete dissolution of NiO_x and FeO_x, which may be the cause of deactivation. From

DOI: 10.1021/acscatal.7b04340
ACS Catal. 2018, 8, 4278−4287

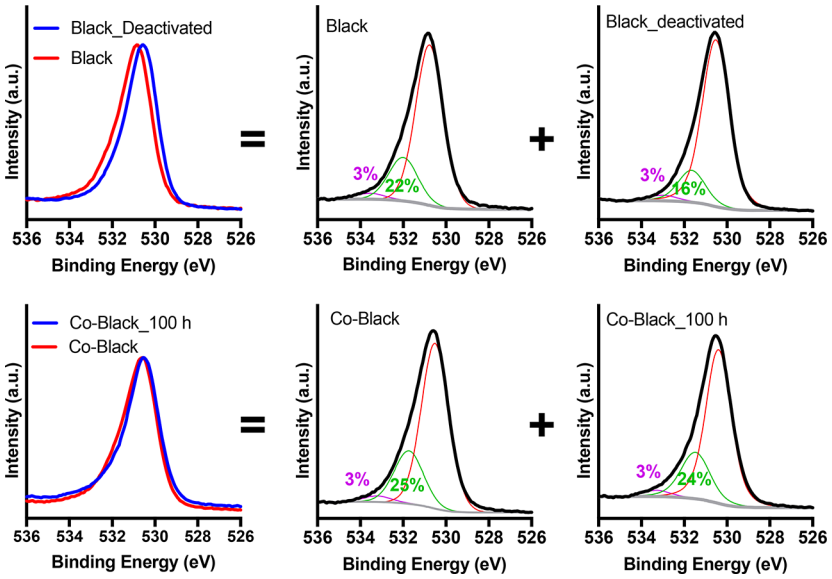

Figure 6. Comparison and peak deconvolutions of O 1s XPS spectra of Black and Co-Black NTA before and after long-term electrolysis.

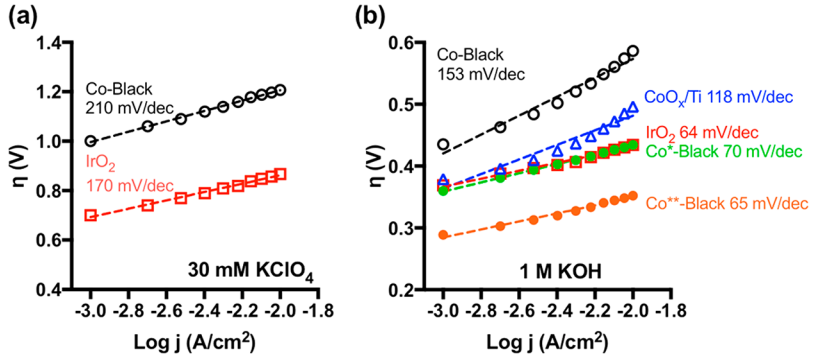

Figure 7. Tafel plots in different electrolytes. Co*- and Co**-Black were prepared by drop-casting 250 mM $Co(NO_3)_2$/ethanol precursor on Co-Black, followed by annealing in 5% H_2/Ar at 450 °C for 30 min. CoO_x/Ti was prepared by the same procedure except that a Ti plate was used as the supporting substrate. The Co loading was 2.1 μmol cm^{-2} for Co*-Black and 4.2 μmol cm^{-2} for Co**-Black and CoO_x/Ti.

a thermodynamic point of view, the Pourbaix diagrams (Figure S2b) also indicate that NiO_x and FeO_x are more vulnerable to corrosion than CoO_x under the conditions of a stability test (2.4−2.7 V_{RHE}, pH 7). These results again highlight the importance of a strong Co−TiO_2 interaction on maintaining the anodic stability of Co-Black NTA electrode.

Two electrochemical applications, the OER and wastewater electrolysis, were tested using the Co-Black electrode. A IrO_2 DSA and a C-DSA with the same geometric surface area were chosen as reference benchmarks, since the DSA-IrO_2 electrode is generally recognized as an inherent standard for both OER and wastewater treatment. Tafel plots (Figure 7 and Figure S11) indicate that Co-Black is less OER active than IrO_2 DSA at both neutral and alkaline pH.

It is found that the OER activity of Co-Black can be enhanced by increasing the Co loading. A $Co(NO_3)_2$/ethanol solution was drop-casted onto a Co-Black electrode. The sample was then reduced in 5% H_2/Ar at 450 °C for 30 min. During annealing, a discrete film layer of amorphous CoO_x formed on top of Co-Black (Figures S12 and S13). The XPS analyses (Figure S14) indicate that the Co of the CoO_x film has higher valence (3+/2+) than that of Co-Black (2+) due to the absence of a Co−TiO_2 interaction. The Co*-Black composite electrode with a Co loading of 2.1 μmol cm^{-2} has over-potentials of 360 and 434 mV, respectively, at 1.0 and 10 mA cm^{-2} in 1 M KOH (Figure 7b). Increasing the Co loading to 4.2 μmol cm^{-2} gave a Co**-Black electrode with an even higher OER activity; this electrode has overpotentials of 289 and 352 mV at 1.0 and 10 mA cm^{-2}, respectively (Figure 7b). The performance of Co**-Black is not only higher than those of IrO_2 DSA, C-DSA, and $Co(OH)_x$/Ti but also superior to the reported activities of a benchmarking $Co(OH)_x$/GC (400 mV at 10 mA cm^{-2}),[27] Co_3O_4 nanowires (320 mV at 1 mA cm^{-2}),[49] Co_3O_4 nanosheets (390 mV at 10 mA cm^{-2}),[46] and Co@Co_3O_4 nanoparticles (420 mV at 10 mA cm^{-2}).[50] A detailed comparison of alkaline OER performance and catalyst parameters is provided in Table S1. The composition of the CoO_x film was not optimized for the OER in this study. It is reasonable to believe that a higher OER activity could be achieved by doping Ni and Fe into the CoO_x film.[51,52]

The higher OER activity of Co**-Black electrode could be attributed to two primary factors. First, more OER active sites are created by the CoO_x film. This effect is illustrated in Figure S15, which shows that the double-layer capacitance, which is proportional to the electrochemically active surface area (ECSA), increases in the order Co-Black (7.5) < Co*-Black (12.4) < Co**-Black (21.4 mF cm^{-2}). Co**-Black with 6 cm^2 geometric area has a large ECSA of 3210 cm^2, giving a

DOI: 10.1021/acscatal.7b04340
ACS Catal. 2018, 8, 4278−4287

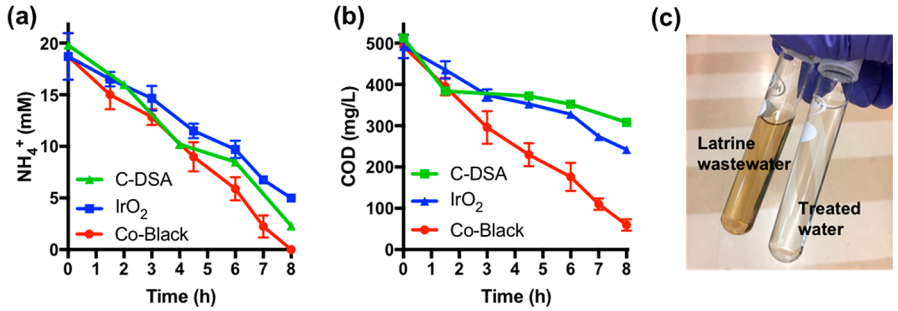

Figure 8. Decay of (a) COD and (b) NH_4^+ as a function of electrolysis time. (c) Photo of wastewater before and after electrolysis.

roughness factor of 535 (Table S1). As shown in Figure S14, XPS analyses prove that Co**-Black has a higher O_v concentration (32%) than Co-Black (25%). The O_vs of CoO_x are surrounded by Co ions (Co−O_v−Co),[45,46] which should be intrinsically more OER active than the Co−O_v−Ti and Ti−O_v−Ti sites of Co-Black. Second, the antipassivation functionality of Co-Black facilitates charge transport from the CoO_x film to Co-Black NTA and then to the Ti metal support underneath. For comparison, CoO_x was directly loaded onto a Ti plate (CoO_x/Ti) and the corresponding OER activity was determined. Even though the Ti substrate has a higher conductivity in comparison to Co-Black (Figure S7), the CoO_x/Ti composite electrode was found to has a lower OER activity in comparison to the Co**-Black electrode (Figure 7b). As illustrated in Figure S16, Co**-Black is stable for more than 200 h in 1.0 M KOH at 10 mA cm^{-2}. In contrast, a gradual deactivation is observed for CoO_x/Ti. Overall, these results indicate that the presence of Co-Black NTA as an interlayer prevents the passivation of the catalyst/Ti interface, which is a major challenge affecting the stability of DSA electrodes.[53]

Although the Co-Black electrode is relatively inert with respect to the OER in comparison to a conventional IrO_2 DSA, it is found to be more active for the electrochemical production of reactive oxygen species and other oxidants (i.e., reactive chlorine species). Electrolysis of a 30 mM NaCl solution shows that Co-Black has a higher chlorine evolution rate (CER) than IrO_2 DSA (Figure S17a). Using benzoic acid and oxalate ion as probe molecules, we show that Co-Black outperforms an IrO_2 DSA in terms of hydroxyl radical (•OH) generation and direct electron transfer oxidation (Figure S17b,c).

Co-Black was further applied for the treatment of latrine wastewater that was collected on the Caltech campus in a prototype solar toilet system.[26,54] Chloride (40 mM) that originated from human waste (i.e., urine) is oxidized to chlorine (e.g., HOCl, ClO^-). Hypochlorous acid, HOCl, reacts with ammonia (NH_3/NH_4^+) to form chloramines (e.g., NH_2Cl, $NHCl_2$), which in turn undergo a self-reaction leading to denitrification with the offgassing of N_2 leading eventually to breakpoint chlorination.[26,54] Co-Black outperforms the IrO_2 DSA due to its higher CER activity (Figure 8a). Although C-DSA has a higher CER (Figure S17), it still exhibits inferior NH_4^+ removal performance in comparison to Co-Black. This is probably because Co-Black is more active for the removal of organics, which compete with NH_4^+ to react with chlorine. Both chlorine and •OH contribute to the removal of organic pollutants (indexed in terms of chemical oxygen demand, COD). As expected, the COD removal capability of Co-Black is superior to that of IrO_2 DSA and C-DSA (Figure 8b). The effluent after 8 h of treatment is clear in appearance and suitable for nonpotable water reuse (Figure 8c).

CONCLUSIONS

In conclusion, the results of this study show that Co doping significantly extends the lifetime of Black NTA electrodes via tuning of the concentration and stability of oxygen vacancies, O_v. Co-Black electrodes are shown to be effective in terms of electrochemical oxidation. Co-Black electrodes also function as the conductive substrates for CoO_x-based OER catalysts. The simplicity of the synthetic procedures suggests that conductive TiO_2 NTA could be utilized for energy storage and industrial applications on a wider scale, provided that the operational lifetimes can be extended further.

ASSOCIATED CONTENT

Supporting Information

The Supporting Information is available free of charge on the ACS Publications website at DOI: 10.1021/acscatal.7b04340.

Details of DFT calculations and additional results of XRD, XPS, SEM-EDS, TEM, two-point solid state measurements, EIS, stability tests, and activity evaluation (PDF)

AUTHOR INFORMATION

Corresponding Author

*E-mail for M.R.H.: mrh@caltech.edu.

ORCID

Yang Yang: 0000-0003-3767-8029
Yuanyue Liu: 0000-0002-5880-8649
Jinghua Guo: 0000-0002-8576-2172

Notes

The authors declare no competing financial interest.

ACKNOWLEDGMENTS

This research was supported by the Bill and Melinda Gates Foundation (BMGF RTTC Grants OPP1111246 and OPP1149755). We also used the resources of the Advanced Light Source, which is a DOE Office of Science User Facility under contract no. DE-AC02-05CH11231. This work benefited from the use of the TEM facility of Applied Physics and Materials Science Department at Caltech. We acknowledge the National Science Foundation for its support of the Caltech EPR Facility via NSF-1531940. We are grateful to Dr. Paul Oyala from the Division of Chemistry and Chemical Engineering of Caltech for help with the EPR measurements and data interpretation.

DOI: 10.1021/acscatal.7b04340
ACS Catal. 2018, 8, 4278−4287

REFERENCES

(1) Hoffmann, M. R.; Martin, S. T.; Choi, W.; Bahnemann, D. W. Environmental Applications of Semiconductor Photocatalysis. *Chem. Rev.* **1995**, *95*, 69−96.

(2) Fujishima, A.; Honda, K. Electrochemical Photolysis of Water at a Semiconductor Electrode. *Nature* **1972**, *238*, 37−38.

(3) Kesselman, J. M.; Weres, O.; Lewis, N. S.; Hoffmann, M. R. Electrochemical Production of Hydroxyl Radical at Polycrystalline Nb-doped TiO_2 Electrodes and Estimation of the Partitioning between Hydroxyl Radical and Direct Hole Oxidation Pathways. *J. Phys. Chem. B* **1997**, *101*, 2637−2643.

(4) Song, Y. Y.; Roy, P.; Paramasivam, I.; Schmuki, P. Voltage-Induced Payload Release and Wettability Control on TiO_2 and TiO_2 Nanotubes. *Angew. Chem., Int. Ed.* **2010**, *49*, 351−354.

(5) Chen, X.; Liu, L.; Peter, Y. Y.; Mao, S. S. Increasing Solar Absorption for Photocatalysis With Black Hydrogenated Titanium Dioxide Nanocrystals. *Science* **2011**, *331*, 746−750.

(6) Naldoni, A.; Allieta, M.; Santangelo, S.; Marelli, M.; Fabbri, F.; Cappelli, S.; Bianchi, C. L.; Psaro, R.; Dal Santo, V. Effect of Nature and Location of Defects on Bandgap Narrowing in Black TiO_2 Nanoparticles. *J. Am. Chem. Soc.* **2012**, *134*, 7600−7603.

(7) Wang, G.; Wang, H.; Ling, Y.; Tang, Y.; Yang, X.; Fitzmorris, R. C.; Wang, C.; Zhang, J. Z.; Li, Y. Hydrogen-Treated TiO_2 Nanowire Arrays for Photoelectrochemical Water Splitting. *Nano Lett.* **2011**, *11*, 3026−3033.

(8) Chen, X.; Liu, L.; Huang, F. Black Titanium Dioxide (TiO_2) Nanomaterials. *Chem. Soc. Rev.* **2015**, *44*, 1861−1885.

(9) Zhou, X.; Liu, N.; Schmuki, P. Photocatalysis with TiO_2 Nanotubes:"Colorful" Reactivity and Designing Site-Specific Photocatalytic Centers into TiO_2 Nanotubes. *ACS Catal.* **2017**, *7*, 3210−3235.

(10) Walsh, F.; Wills, R. The Continuing Development of Magnéli Phase Titanium Sub-Oxides and Ebonex® Electrodes. *Electrochim. Acta* **2010**, *55*, 6342−6351.

(11) Chaplin, B. P. Critical Review of Electrochemical Advanced Oxidation Processes for Water Treatment Applications. *Environ. Sci. Process. Impacts* **2014**, *16*, 1182−1203.

(12) Zaky, A. M.; Chaplin, B. P. Porous Substoichiometric TiO_2 Anodes as Reactive Electrochemical Membranes for Water Treatment. *Environ. Sci. Technol.* **2013**, *47*, 6554−6563.

(13) Kolbrecka, K.; Przyluski, J. Sub-Stoichiometric Titanium Oxides as Ceramic Electrodes for Oxygen Evolution: Structural Aspects of The Voltammetric Behaviour of Ti_nO_{2n-1}. *Electrochim. Acta* **1994**, *39*, 1591−1595.

(14) Mohajernia, S.; Hejazi, S.; Mazare, A.; Nguyen, N. T.; Schmuki, P. Photoelectrochemical H_2 Generation from Suboxide TiO_2 Nanotubes: Visible Light Absorption versus Conductivity. *Chem. - Eur. J.* **2017**, *23*, 12406−12411.

(15) Liu, N.; Häublein, V.; Zhou, X.; Venkatesan, U.; Hartmann, M.; Mackovic, M.; Nakajima, T.; Spiecker, E.; Osvet, A.; Frey, L. Black" TiO_2 Nanotubes Formed by High-Energy Proton Implantation Show Noble-Metal-Co-Catalyst Free Photocatalytic H_2-Evolution. *Nano Lett.* **2015**, *15*, 6815−6820.

(16) Fabregat-Santiago, F.; Barea, E. M.; Bisquert, J.; Mor, G. K.; Shankar, K.; Grimes, C. A. High Carrier Density and Capacitance in TiO_2 Nanotube Arrays Induced by Electrochemical Doping. *J. Am. Chem. Soc.* **2008**, *130*, 11312−11316.

(17) Zhang, Z.; Hedhili, M. N.; Zhu, H.; Wang, P. Electrochemical Reduction Induced Self-Doping of Ti^{3+} for Efficient Water Splitting Performance on TiO_2 Based Photoelectrodes. *Phys. Chem. Chem. Phys.* **2013**, *15*, 15637−15644.

(18) Chang, X.; Thind, S. S.; Chen, A. Electrocatalytic Enhancement of Salicylic Acid Oxidation at Electrochemically Reduced TiO_2 Nanotubes. *ACS Catal.* **2014**, *4*, 2616−2622.

(19) Kim, C.; Kim, S.; Choi, J.; Lee, J.; Kang, J. S.; Sung, Y.-E.; Lee, J.; Choi, W.; Yoon, J. Blue TiO_2 Nanotube Array as an Oxidant Generating Novel Anode Material Fabricated by Simple Cathodic Polarization. *Electrochim. Acta* **2014**, *141*, 113−119.

(20) Yang, Y.; Hoffmann, M. R. Synthesis and Stabilization of Blue-Black TiO_2 Nanotube Arrays for Electrochemical Oxidant Generation and Wastewater Treatment. *Environ. Sci. Technol.* **2016**, *50*, 11888−11894.

(21) Kim, C.; Kim, S.; Hong, S. P.; Lee, J.; Yoon, J. Effect Of Doping Level of Colored TiO_2 Nanotube Arrays Fabricated by Electrochemical Self-Doping on Electrochemical Properties. *Phys. Chem. Chem. Phys.* **2016**, *18*, 14370−14375.

(22) Minguzzi, A.; Fan, F.-R. F.; Vertova, A.; Rondinini, S.; Bard, A. J. Dynamic Potential-pH Diagrams Application to Electrocatalysts for Water Oxidation. *Chem. Sci.* **2012**, *3*, 217−229.

(23) Lutterman, D. A.; Surendranath, Y.; Nocera, D. G. A Self-Healing Oxygen-Evolving Catalyst. *J. Am. Chem. Soc.* **2009**, *131*, 3838−3839.

(24) Paulose, M.; Shankar, K.; Yoriya, S.; Prakasam, H. E.; Varghese, O. K.; Mor, G. K.; Latempa, T. A.; Fitzgerald, A.; Grimes, C. A. Anodic Growth of Highly Ordered TiO_2 Nanotube Arrays to 134 μm in Length. *J. Phys. Chem. B* **2006**, *110*, 16179−16184.

(25) Yu, D.; Zhu, X.; Xu, Z.; Zhong, X.; Gui, Q.; Song, Y.; Zhang, S.; Chen, X.; Li, D. A Facile Method to Enhance the Adhesion of TiO_2 Nanotube Arrays to Ti Substrate. *ACS Appl. Mater. Interfaces* **2014**, *6*, 8001−8005.

(26) Yang, Y.; Shin, J.; Jasper, J. T.; Hoffmann, M. R. Multilayer Heterojunction Anodes for Saline Wastewater Treatment: Design Strategies and Reactive Species Generation Mechanisms. *Environ. Sci. Technol.* **2016**, *50*, 8780−8787.

(27) McCrory, C. C.; Jung, S.; Peters, J. C.; Jaramillo, T. F. Benchmarking Heterogeneous Electrocatalysts for the Oxygen Evolution Reaction. *J. Am. Chem. Soc.* **2013**, *135*, 16977−16987.

(28) Huang, B.; Yang, W.; Wen, Y.; Shan, B.; Chen, R. Co_3O_4-Modified TiO_2 Nanotube Arrays via Atomic Layer Deposition for Improved Visible-Light Photoelectrochemical Performance. *ACS Appl. Mater. Interfaces* **2015**, *7*, 422−431.

(29) Pozio, A. Effect of Low Cobalt Loading on TiO_2 Nanotube Arrays for Water-Splitting. *Int. J. Electrochem.* **2014**, *2014*, 1.

(30) Liu, Q.; Ding, D.; Ning, C.; Wang, X. Cobalt-Phosphate/Ni-Doped TiO_2 Nanotubes Composite Photoanodes for Solar Water Oxidation. *Mater. Sci. Eng., B* **2015**, *202*, 54−60.

(31) Tsui, L.-k.; Xu, Y.; Dawidowski, D.; Cafiso, D.; Zangari, G. Efficient Water Oxidation Kinetics and Enhanced Electron Transport in Li-Doped TiO_2 Nanotube Photoanodes. *J. Mater. Chem. A* **2016**, *4*, 19070−19077.

(32) Zhang, K.; Lin, L.; Li, L.; Pan, S.; Wu, P.; Li, X.; Liu, A.; Zhang, H. Cobalt Doped Titanate Nanotubes: Synthesis and Properties. *Wuhan Univ. J. Nat. Sci.* **2017**, *22*, 201−206.

(33) Kanan, M. W.; Nocera, D. G. In Situ Formation of an Oxygen-Evolving Catalyst in Neutral Water Containing Phosphate and Co^{2+}. *Science* **2008**, *321*, 1072−1075.

(34) Kanan, M. W.; Surendranath, Y.; Nocera, D. G. Cobalt-Phosphate Oxygen-Evolving Compound. *Chem. Soc. Rev.* **2009**, *38*, 109−114.

(35) Chen, C. L.; Dong, C.-L.; Chen, C.-H.; Wu, J.-W.; Lu, Y.-R.; Lin, C.-J.; Liou, S. Y. H.; Tseng, C.-M.; Kumar, K.; Wei, D.-H. Electronic Properties of Free-Standing TiO_2 Nanotube Arrays Fabricated by Electrochemical Anodization. *Phys. Chem. Chem. Phys.* **2015**, *17*, 22064−22071.

(36) Henderson, G.; Liu, X.; Fleet, M. A Ti L-Edge X-Ray Absorption Study of Ti-Silicate Glasses. *Phys. Chem. Miner.* **2002**, *29*, 32−42.

(37) Li, J.; Liu, C.-H.; Li, X.; Wang, Z.-Q.; Shao, Y.-C.; Wang, S.-D.; Sun, X.-L.; Pong, W.-F.; Guo, J.-H.; Sham, T.-K. Unraveling the Origin of Visible Light Capture by Core-Shell TiO_2 Nanotubes. *Chem. Mater.* **2016**, *28*, 4467−4475.

(38) Li, J.; Wang, Z.; Wang, J.; Sham, T.-K. Unfolding The Anatase-To-Rutile Phase Transition in TiO_2 Nanotubes Using X-Ray Spectroscopy and Spectromicroscopy. *J. Phys. Chem. C* **2016**, *120*, 22079−22087.

(39) Kang, W.; Spanjers, C. S.; Rioux, R. M.; Hoefelmeyer, J. D. Synthesis of Brookite TiO_2 Nanorods with Isolated Co (II) Surface

DOI: 10.1021/acscatal.7b04340
ACS Catal. 2018, 8, 4278−4287

Sites and Photocatalytic Degradation of 5, 8-Dihydroxy-1, 4-Naphthoquinone Dye. *J. Mater. Chem. A* **2013**, *1*, 7717−7728.
(40) Pan, X.; Yang, M.-Q.; Fu, X.; Zhang, N.; Xu, Y.-J. Defective TiO_2 with Oxygen Vacancies: Synthesis, Properties and Photocatalytic Applications. *Nanoscale* **2013**, *5*, 3601−3614.
(41) Schmidt, J. G.; Brey, W. S., Jr; Stoufer, R. C. Complexes of Cobalt (II). IV. Electron Paramagnetic Resonance Spectra of Some Magnetically Anomalous Complexes of Cobalt (II). *Inorg. Chem.* **1967**, *6*, 268−271.
(42) Conesa, J.; Soria, J. Reversible Titanium (3+) Formation by Hydrogen Adsorption on M/Anatase (TiO_2) Catalysts. *J. Phys. Chem.* **1982**, *86*, 1392−1395.
(43) Hardin, W. G.; Mefford, J. T.; Slanac, D. A.; Patel, B. B.; Wang, X.; Dai, S.; Zhao, X.; Ruoff, R. S.; Johnston, K. P.; Stevenson, K. J. Tuning the Electrocatalytic Activity of Perovskites through Active Site Variation and Support Interactions. *Chem. Mater.* **2014**, *26*, 3368−3376.
(44) Zhu, Y.; Zhou, W.; Yu, J.; Chen, Y.; Liu, M.; Shao, Z. Enhancing Electrocatalytic Activity of Perovskite Oxides by Tuning Cation Deficiency for Oxygen Reduction and Evolution Reactions. *Chem. Mater.* **2016**, *28*, 1691−1697.
(45) Zhuang, L.; Ge, L.; Yang, Y.; Li, M.; Jia, Y.; Yao, X.; Zhu, Z. Ultrathin Iron-Cobalt Oxide Nanosheets with Abundant Oxygen Vacancies for the Oxygen Evolution Reaction. *Adv. Mater.* **2017**, *29*, 1606793.
(46) Bao, J.; Zhang, X.; Fan, B.; Zhang, J.; Zhou, M.; Yang, W.; Hu, X.; Wang, H.; Pan, B.; Xie, Y. Ultrathin Spinel-Structured Nanosheets Rich in Oxygen Deficiencies for Enhanced Electrocatalytic Water Oxidation. *Angew. Chem.* **2015**, *127*, 7507−7512.
(47) Zhu, K.; Neale, N. R.; Miedaner, A.; Frank, A. J. Enhanced Charge-Collection Efficiencies and Light Scattering in Dye-Sensitized Solar Cells Using Oriented TiO_2 Nanotubes Arrays. *Nano Lett.* **2007**, *7*, 69−74.
(48) Jain, A.; Ong, S. P.; Hautier, G.; Chen, W.; Richards, W. D.; Dacek, S.; Cholia, S.; Gunter, D.; Skinner, D.; Ceder, G.; Persson, K. A. Commentary: The Materials Project: A Materials Genome Approach to Accelerating Materials Innovation. *APL Mater.* **2013**, *1*, 011002.
(49) Wang, Y.; Zhou, T.; Jiang, K.; Da, P.; Peng, Z.; Tang, J.; Kong, B.; Cai, W. B.; Yang, Z.; Zheng, G. Reduced Mesoporous Co_3O_4 Nanowires as Efficient Water Oxidation Electrocatalysts and Supercapacitor Electrodes. *Adv. Energy Mater.* **2014**, *4*, 1400696.
(50) Aijaz, A.; Masa, J.; Rösler, C.; Xia, W.; Weide, P.; Botz, A. J.; Fischer, R. A.; Schuhmann, W.; Muhler, M. Co@ Co_3O_4 Encapsulated in Carbon Nanotube-Grafted Nitrogen-Doped Carbon Polyhedra as an Advanced Bifunctional Oxygen Electrode. *Angew. Chem., Int. Ed.* **2016**, *55*, 4087−4091.
(51) Smith, R. D.; Prévot, M. S.; Fagan, R. D.; Zhang, Z.; Sedach, P. A.; Siu, M. K. J.; Trudel, S.; Berlinguette, C. P. Photochemical Route for Accessing Amorphous Metal Oxide Materials for Water Oxidation Catalysis. *Science* **2013**, *340*, 60−63.
(52) Bates, M. K.; Jia, Q.; Doan, H.; Liang, W.; Mukerjee, S. Charge-Transfer Effects in Ni−Fe and Ni−Fe−Co Mixed-Metal Oxides for the Alkaline Oxygen Evolution Reaction. *ACS Catal.* **2016**, *6*, 155−161.
(53) Spoeri, C.; Kwan, J. T. H.; Bonakdarpour, A.; Wilkinson, D.; Strasser, P. The Stability Challenges of Oxygen Evolving Electrocatalysts: Towards a Common Fundamental Understanding and Mitigation of Catalyst Degradation. *Angew. Chem., Int. Ed.* **2017**, *56*, 5994−6021.
(54) Cho, K.; Kwon, D.; Hoffmann, M. R. Electrochemical Treatment of Human Waste Coupled with Molecular Hydrogen Production. *RSC Adv.* **2014**, *4*, 4596−4608.

DOI: 10.1021/acscatal.7b04340
ACS Catal. 2018, 8, 4278−4287